Magnetic Manipulation of Superparamagnetic Colloids in Droplet-Based Optical Devices

Iacopo Mattich, Joan Sendra, Henning Galinski, Golnaz Isapour, Ahmet F. Demirörs, Marco Lattuada, Simone Schuerle, and André R. Studart*

Magnetically assembled superparamagnetic colloids are exploited as fluid mixers, swimmers, and delivery systems in several microscale applications. The encapsulation of such colloids in droplets may open new opportunities to build magnetically controlled displays and optical components. Here, the assembly of superparamagnetic colloids inside droplets under rotating magnetic fields is studied, and this phenomenon is exploited to create functional optical devices. Colloids are encapsulated in monodisperse droplets produced by microfluidics and magnetically assembled into dynamic 2D clusters. Using an optical microscope equipped with a magnetic control setup, the effect of the magnetic field strength and rotational frequency on the size, stability, and dynamics of 2D colloidal clusters inside droplets is investigated. The results show that cluster size and stability depend on the magnetic forces acting on the structure under the externally imposed field. By rotating the cluster in specific orientations, it is possible to magnetically control the effective refractive index and the transmission of light through the colloid-laden droplets, thus demonstrating the potential of the encapsulated colloids in optical applications.

1. Introduction

Magnetic fields offer a powerful means to assemble or manipulate colloids for a broad range of fields, from microrobotics to medicine, biotechnology, and manufacturing.[1–4] In microrobotics, magnetic stimuli have been used to control the locomotion of miniaturized robots[1,5] and to design substrates for the remote manipulation of small-scale objects.[6–8] Locally induced hyperthermia and directed transport using iron oxide particles are well-known examples of potential applications in medicine, in which a magnetic stimulus is employed as a non-invasive tool for drug delivery and cancer therapy.[2,9] In manufacturing, magnetic fields have been exploited for the fabrication of composites with controlled orientation of reinforcing particles[3,10] or the formulation of reversible adhesives.[11] Moreover, analytical biotechnological assays often rely on magnetic fields to recover surface-functionalized colloids in biological and chemical separation processes.[4,12] In many of these applications, superparamagnetic iron oxide nanoparticles (SPIONs) are used as the magnetically responsive colloids.[9]

Suspensions of superparamagnetic particles exhibit very rich phase behavior and dynamics when subjected to time-varying magnetic fields.[13,14] Their main advantage lies on the fact

I. Mattich, A. F. Demirörs, A. R. Studart
Complex Materials
Department of Materials
ETH Zürich
Zürich 8093, Switzerland
E-mail: andre.studart@mat.ethz.ch

J. Sendra, H. Galinski
Laboratory for Nanometallurgy
Department of Materials
ETH Zürich
Zürich 8093, Switzerland

G. Isapour
Department of Mechanical Engineering
MIT
Cambridge MA 02139, USA

M. Lattuada
Department of Chemistry
University of Fribourg
Fribourg 1700, Switzerland

S. Schuerle
Department of Health Sciences and Technology
Institute for Translational Medicine
ETH Zürich
Zürich 8093, Switzerland

ADVANCED
SCIENCE NEWS

www.advancedsciencenews.com

ADVANCED
OPTICAL
MATERIALS

www.advopticalmat.de

that these particles act as magnetic dipoles exhibiting a single magnetic domain only in the presence of an external magnetic field. This allows for switching the colloidal state of the suspension from a fluid dispersion to hierarchical assemblies of particles interacting through attractive and repulsive dipolar forces. Depending on the concentration of particles and the type of magnetic stimulus applied, superparamagnetic colloids can assemble into chains, 2D clusters or 3D hierarchical networks.[13] Such colloidal structures have been considered for several prospective applications as microfluidic mixers,[15] microswimmers, micropumps,[16] cargo transporters,[17] and artificial ciliated surfaces.[13,18] Despite these potential applications and our advanced understanding of their magnetic response, the directed assembly of superparamagnetic particles compartmentalized inside droplets remains to be investigated and technologically exploited.

The compartmentalization of colloidal particles inside droplets and capsules is an effective approach to control the release of molecules in delivery systems[19] and to program the brightness of pixels in commercially available electronic books.[20,21] In electronic paper, the encapsulated particles are manipulated using an external electrical field to change optical properties locally across large areas. The applied electrical field drives the motion of black and white encapsulated particles of opposite charges to different regions of the capsule, thus allowing for electrical control of the local brightness.[20] In nature, pigment granules compartmentalized in chromatophore cells are also used by cephalopods to change color on demand.[22,23] In this case, color is generated through the displacement of granules via controlled contraction or expansion of encapsulating sacks.[22] Such a strategy has inspired the development of magnetically controlled smart windows.[24] These biological and technological examples demonstrate the potential of controlled colloidal manipulation in compartments as an enticing approach to create novel functionalities. Given the increasing availability of multiferroic materials that can generate magnetic fields using low-power electrical input,[25,26] the use of magnetic torques and forces to drive and control the assembly of colloids in droplets is an interesting and technologically relevant approach that calls for further scientific research.

Here, we study the assembly and manipulation of superparamagnetic colloids inside droplets driven by a time-varying external magnetic field. The magnetically responsive colloids are encapsulated in water-in-oil droplets through a microfluidic emulsification approach. After encapsulation in monodisperse droplets, the particles are assembled and manipulated using a tunable rotating magnetic field. In contrast to bulk suspensions, the compartmentalization in droplets allows for control over the number of assembled particles and the size of the resulting clusters. Next, the response of the colloids to the external field is studied by optical microscopy imaging of multiple droplet arrays. Finally, we demonstrate how superparamagnetic particles in droplets can be potentially exploited as magnetically controlled optical shutters and microlens arrays with tunable focal length.

2. Results and Discussion

The assembly of colloids under rotating magnetic fields is experimentally studied by encapsulating monodisperse colloidal particles inside monodisperse water droplets suspended in a continuous oil phase (**Figure 1**). The colloids consist of polystyrene particles with an average size of 480 nm loaded with SPIONs (10–20 nm) to render them magnetically responsive. Due to the high density of carboxylic acid groups (COOH) on the surface (>50 μmol g^{-1}), the particles become negatively charged in water at neutral and alkaline pHs. 1-decanol is used as the continuous phase, whereas the aqueous droplet is prepared from double deionized water. The concentration of colloidal particles inside the droplet is varied between 0.01 and 0.78 vol% to generate clusters that are large enough for visualization by optical microscopy while keeping the system sufficiently diluted to facilitate assembly.

To study the assembly of the particles into 2D clusters, we apply a time-varying external magnetic field to a monolayer of colloid-laden droplets using two types of magnetic stimuli (Figure 1a–c). In a first approach, an external magnetic field is used to drive the assembly of 2D colloidal clusters. To this end, the applied field is rotated within the plane orthogonal to the viewing direction (xy-plane), thus facilitating visualization of the cluster assembly process. In a second step, the same rotating magnetic field is first used to form the 2D clusters and is then employed to manipulate the colloidal assembly within the droplet. This manipulation is accomplished by applying the rotating field in a plane parallel to the viewing angle and revolving it around the viewing axis to rotate the 2D colloidal cluster. To study the dynamics of the colloidal assembly process and the magnetic manipulation of the resulting clusters, the droplets need to be sufficiently stable against coalescence and coarsening events.

Monodisperse, stable droplets were generated in a flow-focusing microfluidic device using Pickering emulsions as templates (Figure 1d–h). The Pickering emulsions were formed by adsorbing silica nanoparticles at the water–oil interface. In this microfluidic emulsification approach, water droplets are formed in a continuous oil phase through a flow-induced dripping mechanism.[27] Emulsification occurs by injecting the aqueous inner phase and the oil outer phase through separate input channels of the microfluidic device (Figure 1d). The channels are designed to form an aperture, at which the dripping phenomenon takes place (Figure 1g). The aqueous inner phase consists of a suspension of superparamagnetic colloidal particles in water, whereas 1-decanol is used as the outer oil phase.

To facilitate the Pickering stabilization of the oil–water interface, a second coaxial aqueous phase is added in the device during emulsification. Such liquid phase comprises the silica nanoparticles suspended in water and is injected alongside the innermost aqueous phase in a co-flow configuration. Such an approach enables the delivery of the silica nanoparticles very close to the oil–water interface formed upon dripping. The silica nanoparticles were partially hydrophobized with hexyl amine to favor their adsorption at the oil–water interface. Interfacial adsorption of the silica particles is aided by a silicone-based surfactant (ABIL 90 EM) added to the oil phase.

Droplet microfluidics enabled precise control over the emulsion droplet size, monodispersity, droplet surface coverage, and concentration of encapsulated superparamagnetic particles. By tuning the concentration of surfactant and modified silica nanoparticles, stable Pickering emulsions were obtained at the
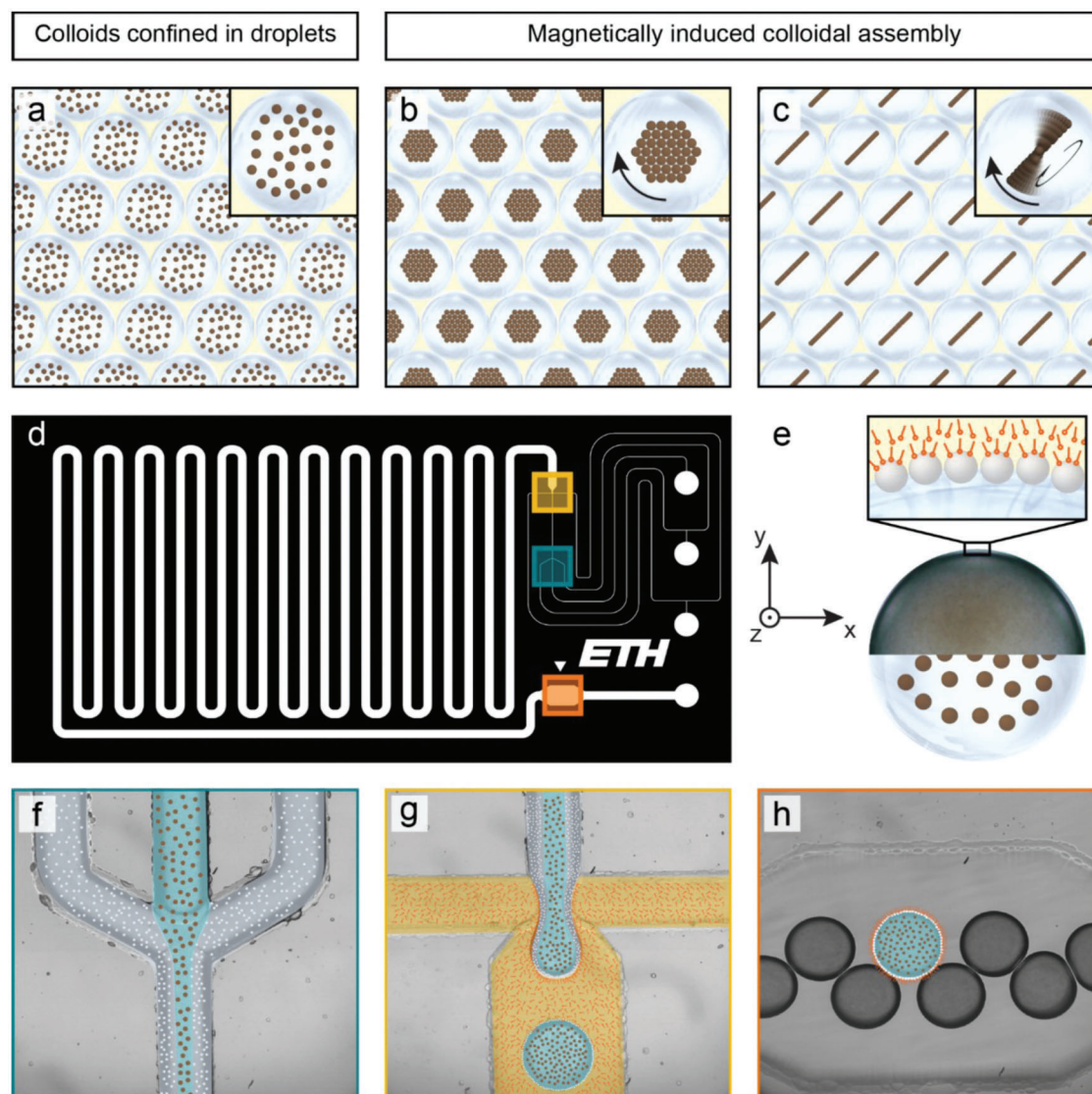
**ADVANCED
SCIENCE NEWS**

www.advancedsciencenews.com

**ADVANCED
OPTICAL
MATERIALS**

www.advopticalmat.de

Figure 1. Microfluidic encapsulation and magnetically driven assembly of colloidal particles inside droplets. a) Illustration of colloids loaded with superparamagnetic polystyrene particles confined in water-in-oil droplets. When no magnetic field is applied, the colloidal particles undergo random Brownian motion. b) Schematic of the assembly of colloidal particles into large 2D clusters under a rotating magnetic field with a frequency $f_{formation}$ of 125 Hz applied within the xy-plane. c) After cluster formation, the axis of rotation of the rotating field can be slowly adjusted until it lies parallel to the y-axis, thus shifting the color of the droplet from dark to translucent. At this point, the rotating field plane is revolved around the z-axis at a certain pre-defined speed to study the mechanical stability of the cluster. d) Overview of the flow-focusing microfluidic device, highlighting the junctions and chamber where droplets are formed and collected. e) Cartoon illustrating the stabilization of the water–oil interface by surface-modified silica nanoparticles and surfactant molecules. f) Magnification of the first junction, indicating the laminar co-flow of the aqueous phases containing the superparamagnetic colloids (center) and the silica nanoparticles (close to walls). g) Magnification of the second junction, where water-in-oil droplets are formed by flow-induced dripping. h) Magnification of the observation chamber at the end of the serpentine channel. The droplets are stable and do not coalesce upon physical contact. The particles, fluids, and surfactants were false-colored in the images to facilitate visualization.

end of the serpentine channel and outside of the microfluidic device. This high stability was crucial to study the assembly and manipulation of the encapsulated superparamagnetic polystyrene particles using an external magnetic field. Due to this high stability, no variation in droplet size is observed within the timeframe of our experiments. In addition to droplet stability, the silica particles adsorbed at the oil–water interface prevented leakage of the encapsulated superparamagnetic colloids to the continuous phase.

Magnetic fields with a rotational frequency ($f_{formation}$) of 125 Hz were applied to a monolayer of droplets to study the assembly and manipulation of colloidal clusters (**Figure 2**). Because of their negative surface charges, the colloids are initially electrostatically stabilized and uniformly dispersed within the droplets (Figure 2a). The use of a magnetic setup with eight electromagnetic coils and five degrees of freedom[28,29] allowed us to gain full control over the magnetic field applied to the colloidal particles. Comparative experiments with particles suspended
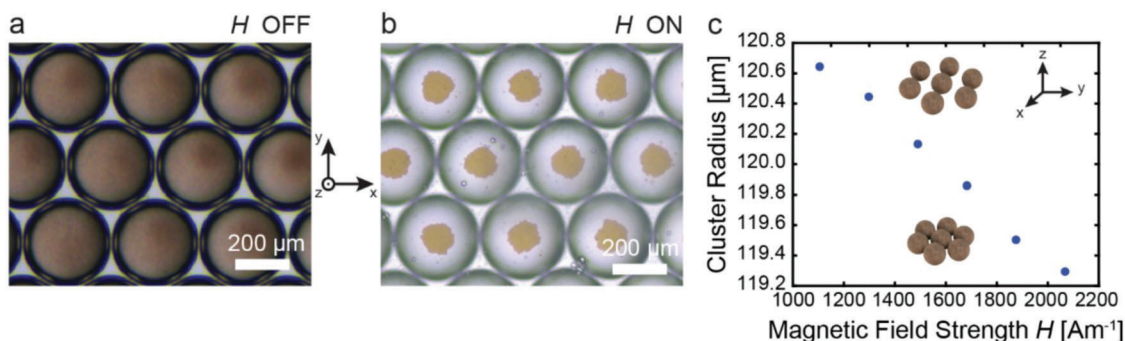
Figure 2. Magnetic assembly of superparamagnetic particles into 2D colloidal clusters inside droplets. a) Optical microscopy image of an array of monodisperse water-in-oil droplets with superparamagnetic particles homogeneously suspended in the aqueous phase. b) Particles assemble into 2D clusters when a magnetic field (H) of 1887.4 Am^{-1} rotating at 125 Hz is applied within the xy-plane. c) Effect of the magnetic field strength (H) on the diameter ($2R$) of the assembled colloidal clusters. The concentration of the magnetic polystyrene particles suspension is 0.1061 vol%.

in water showed that their encapsulation inside droplets is crucial to prevent cluster–cluster interactions and thus allow for the systematic investigation of the assembly and dynamics of individual 2D clusters. The high monodispersity of the droplets led to crystallization in ordered domains, thereby facilitating the imaging of the colloidal assembly process in multiple droplets simultaneously.

Our experiments revealed that the initially dispersed colloidal particles readily assemble into 2D clusters when subjected to a rotating magnetic flux density (B) with amplitude in the range of 6–11 mT and a high frequency ($f_{formation}$) of 125 Hz (Figure 2). The magnitude of the field applied corresponds to a magnetic field strength between 1132 and 2076 A m^{-1}. The assembly process is governed by magnetic interactions between the field-induced magnetic dipoles within individual particles. The superparamagnetic nature of the colloids leads to induced dipoles within the plane of the rotating field, which attract each other to initially form small clusters of colloidal particles. Over time, the small clusters merge into a large 2D assembly with one or two layers of particles, depending on the initial colloid concentration. While the dipole–dipole interactions in the bulk of the cluster cancel each other, the particles positioned at the edge of the cluster experience a net magnetic moment due to the absence of neighboring colloids outside the cluster.[14] The dipolar–dipolar attractive interactions between such particles lead to a line tension (λ), which is a 2D analogue of the surface tension of 3D matter. Such line tension and the interfacial properties of such magnetically assembled clusters have been experimentally measured from fluctuations of surface waves on the perimeter of the clusters[30] or fluctuations in the thickness of particle strips subjected to a rotating magnetic field.[31]

The emergence of a line tension allows us to magnetically control the size and mechanical properties of the assembled cluster. To demonstrate this, we measured the average diameter of the clusters as a function of the applied magnetic field for a constant high frequency ($f_{formation}$) of 125 Hz (Figure 2c). The experiments reveal a linear decrease in the average cluster size with the applied field. This result can be interpreted by analyzing the effect of the magnetically induced line tension on the structure of the colloidal cluster. The line tension arising from the rotating magnetic field pulls the colloidal particles together into a more compact closely packed structure. This compressive force is counteracted by electrostatic and/or steric repulsive forces between adjacent particles, which eventually establish a new equilibrium at smaller interparticle distances.

The smaller distance between colloidal particles affects the mechanical properties of the cluster. At closer distances, stronger interactions are expected between the colloidal particles, enhancing the stiffness of the cluster. To gain an insight into the effect of the magnetic field on the cluster stiffness, we call upon simple scaling relations previously proposed. The shear modulus of the cluster (G'), taken here as a measure of stiffness, can be approximated by λ/R.[14] Earlier work has shown that the line tension λ is expected to scale with the square of the field amplitude: $\lambda \approx H^2$.[14,32] Combining these relations, we conclude that the stiffness of the cluster should scale with the ratio H^2/R, a quantity that can be directly calculated from our experimental data. Our calculations reveal that the H^2/R values range from 36 to 10 A^2 mm^{-2} for the experimentally investigated clusters. Since the cluster size only changes by a few percent, the stiffness is dominated by the applied magnetic field strength, which varies by a factor of $\approx$3.5 between the largest and the smallest clusters. This analysis indicates the possibility of using magnetic fields to control the stiffness of the 2D colloidal clusters.

In addition to the formation of 2D assemblies with controlled size and stiffness, the rotating field can also be used to manipulate the as-formed colloidal clusters encapsulated within the droplets. Manipulation of the dynamically assembled 2D clusters is possible by moving the plane of rotation while keeping the in-plane frequency active (**Figure 3**). To demonstrate such magnetic control capabilities, we performed experiments in which 2D clusters are first assembled with a magnetic field rotating in the xy-plane. Afterward, the axis of rotation of the clusters is turned to become parallel to the y-axis. Finally, their stability is studied by revolving the clusters around the z-axis at increasing angular speeds, starting from 0.1 rad s^{-1} (Figure 3a,b, see Supporting Information). Optical microscopy imaging reveals that the encapsulated clusters can be effectively rotated inside the droplets without losing their 2D morphology. The motion of the cluster into a new orientation changes dramatically the transmittance of light across the droplet and thereby the optical properties of the entire droplet array.
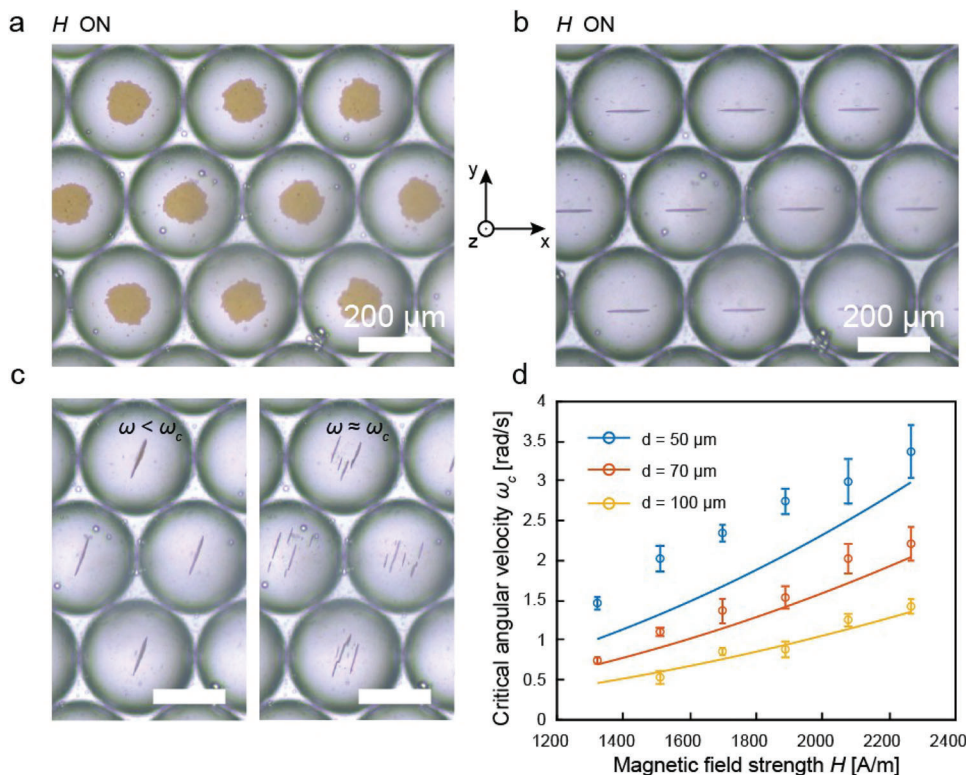
**ADVANCED
SCIENCE NEWS**

www.advancedsciencenews.com

**ADVANCED
OPTICAL
MATERIALS**

www.advopticalmat.de

Figure 3. Manipulation and fragmentation dynamics of magnetically assembled 2D colloidal clusters. a) Optical microscopy image depicting an array of encapsulated clusters formed in the presence of a magnetic field rotating within the *xy*-plane. b) Reorientation of the clusters shown in (a) achieved by turning the axis of rotation around the *x*-axis. c) Fragmentation of the clusters observed when the revolving speed ($\omega_{\text{revolution}}$) of the rotating field is increased above the critical value, ω_{c}. In this experiment, the plane of the rotating magnetic field was revolved around the *z*-axis. d) Effect of the magnetic field strength on the critical revolving speed (ω_{c}) for clusters of different diameters *d*. The continuous lines represent the analytical solution $\omega_{\text{c}} = kH_0^2$, with *k* values calculated from parameters that are known for our system (Table S1, Supporting Information).

The ability of the cluster to remain stable during magnetic manipulation depends on the applied revolving speed ($\omega_{\text{revolution}}$) and the external magnetic field strength (*H*). We experimentally observed that revolving speeds above a critical value (ω_{c}) lead to extensive fragmentation of the 2D clusters into smaller colloidal assemblies (Figure 3c and Movie S1, Supporting Information). To better understand this fragmentation phenomenon, we measured the critical revolving speeds for clusters of different sizes subjected to distinct external rotating magnetic field strengths (Figure 3d). Our results show that the critical revolving speed (ω_{c}) increases with the strength of the rotating field applied (*H*). For a cluster intermediate size of 70 µm, we find that the ω_{c} value doubles when the magnetic field increases from 1321 to 2265 A m^{-1}. Moreover, smaller clusters can be revolved without fragmentation at a higher angular velocity compared to their larger counterparts. Under a magnetic field strength of 673 A m^{-1}, the threshold revolving speed drops from 3.37 to 1.42 rad s^{-1} if the cluster size is enlarged from 50 to 100 µm.

The effect of the magnetic field strength and cluster size on the critical revolving speed (ω_{c}) can be interpreted by considering the forces acting on the cluster during magnetic manipulation. Earlier studies have shown that a balance between the magnetic torque T_{m} arising from the applied field and the reactive viscous torque T_{η} exerted by the liquid governs the dynamics of anisotropic assemblies and particles under rotating magnetic

fields.[13,33,34] For steady-state rotation of our system, a net balance of these forces is achieved such that $T_{\text{m}} + T_{\eta} = 0$, leading to the following expression:

$$\omega_{\text{revolution}} - \omega_{\text{c}} \sin 2\theta = \frac{d\theta}{dt} \tag{1}$$

with

$$\omega_{\text{c}} = \frac{\mu_0 \chi_{\text{cluster}}^2}{12\eta_0 \left(f/f_0\right)\left(1 + \chi_{\text{cluster}}\right)} \cdot H_0^2 \tag{2}$$

Here, θ represents the phase lag between the plane of the rotating magnetic field and the cluster's long axis, while $\omega_{\text{revolution}}$ is the fixed magnetic field angular speed applied. μ_0 indicates the magnetic permeability of free space, χ_{cluster} is the effective magnetic susceptibility of the cluster and H_0 is the applied magnetic field. η_0 is the viscosity of the fluid surrounding the cluster and $\left(f/f_0\right)$ represents the Perrin friction factor. The frequency of rotation of the cluster is coupled with the magnetic field rotational frequency when the phase lag is constant over time ($\frac{d\theta}{dt} = 0$). Assuming that inertial and gravitational effects can be neglected, the anisotropic object will follow the rotating magnetic field if its frequency $\omega_{\text{revolution}}$ lies below the critical value, ω_{c}. When this critical condition is surpassed, the rotating object cannot keep up

**ADVANCED
SCIENCE NEWS**

www.advancedsciencenews.com

**ADVANCED
OPTICAL
MATERIALS**

www.advopticalmat.de

with the speed of the rotating field, resulting in structural instability and loss of synchronous motion.

The theoretical analysis above predicts that the critical angular speed (ω_c) measured in our experiments should scale with the square of the applied magnetic field strength (H_0): $\omega_c = kH_0^2$, with k depending on the particle magnetization, cluster diameter and fluid viscosity (see Supporting Information). Such dependence is analogous to that observed for chains of magnetic particles, clusters, and magnetized platelets under rotating magnetic fields.[3,35–37] For these anisotropic systems, the critical frequency is also controlled by a balance between magnetic and viscous torques.

We test the above prediction by comparing the analytical model derived in Equation (2) to our experimental data (Figure 3d). In this comparison, we estimate the parameter k assuming values for μ_0, $\chi_{cluster}$, η_0, and f/f_0 that are known for our system or available in the literature (Supporting Information). The good agreement observed between experiments and the analytical model suggests that the dynamics of the rotating clusters is captured well by the torque balance proposed in the literature (Figure 3d). The decrease in the k value with increasing cluster size reflects the stronger viscous forces exerted on larger clusters compared to smaller counterparts. This explains the lower critical rotational speeds experimentally needed for the fragmentation of larger clusters. Fragmentation lowers the viscous forces acting on the newly formed smaller clusters, which are stable enough to synchronously rotate with the applied magnetic field (Movie S1, Supporting Information). Catastrophic fragmentation events were more difficult to detect for smaller cluster sizes, because these clusters tended to undergo shear-induced in-plane deformation before catastrophic rupture. This may explain the discrepancy for smaller cluster diameters with our analytical model.

The formation and manipulation of 2D colloidal clusters under a rotating field opens new opportunities to magnetically control the optical properties of individual droplets. The use of magnetic fields to control the refractive index and light transmittance of the droplets can potentially be exploited for the development of active optical components, such as shutters and microlens arrays. Liquid droplets have been shown to be powerful components for the manipulation of light in optical devices[38] as well as inside living cells.[39] To illustrate the potential of our droplet-based system in optical applications, we first study the transmittance of light across monodisperse droplets under magnetic fields and later assemble similar droplets into a polymer matrix to create magnetically controlled soft optical shutters.

In the first demonstrator, a colloid-laden water-in-oil droplet is used as a microlens with magnetically controlled effective refractive index. The effective refractive index is affected by the spatial distribution and assembly of the superparamagnetic colloids inside the droplet. By changing the effective refractive index of the droplet, it is possible to actively control the focal length of the microlens. In contrast to inspiring previous research on droplet-based lenses,[38] the focal length in our demonstrator is actively controlled by the external magnetic field. To quantify this effect, we measured the change in the focal length of a single microlens upon exposure to a magnetic field parallel or perpendicular to the incoming light (**Figure 4**). For these measurements, a table-top optical setup was built around the electro-magnetic coils that

apply the external magnetic field (Figure 4d). A sample holder was 3D printed to host the monolayer of droplets loaded with superparamagnetic colloids (Figure S1, Supporting Information).

For the experiment, a monochromatic collimated laser beam with a wavelength of 532 nm illuminates the sample and the refracted beam intensity profile is mapped around the resulting focal point. To enable the assembly and manipulation of 2D colloidal clusters inside the individual droplets, a magnetic field rotating at 125 Hz was applied following the protocol stated above. Before the magnetic field is applied, the droplet contains a homogeneous dispersion of particles (state 1). The change in focal length of the droplet-based microlens was measured for two magnetically induced conditions: 2D clustering parallel to the input beam (state 2) and 2D clustering perpendicular to the input beam (state 3).

The experimental results show that we can discretely change the focal length depending on the state of the superparamagnetic colloids (Figure 4a–c). Because of the lower refractive index of water compared to the oil, the focal point for all the investigated states is positioned between the light source and the droplet-based microlens. The magnetically induced assembly of dispersed particles into clusters directly affects the experimentally measured focal length. To evaluate this effect, we set as reference the focal length created by droplets with parallel-aligned clusters (state 2, $z = 0$ in Figure 4b) and report the shift in focal length observed when the magnetic field is switched off (state 1, Figure 4a), and when clusters are assembled perpendicular to the incoming light (state 3, Figure 4c). In the reference state 2, the cluster is oriented parallel to the beam and interacts minimally with the incoming light, leading to droplets with optical properties dominated by the aqueous phase. Switching off the field (state 1) leads to thermal randomization of the particles and a shift in focal length of 92 μm. The focal length change reduces to 84 μm, if the cluster is magnetically oriented perpendicular to the input beam (Figure 4b,c).

To establish a quantitative correlation between the change of the microlens focal length and the assembly of superparamagnetic colloids in the droplet, we applied a ray tracing analytical model and finite element simulations to our optical system. Using the transfer matrix method, the analytical model predicts the inverse of the focal length ($1/f$) to depend on the effective refractive index of the droplet, the refractive index of the oil, and the radius of the droplet (see Supporting Information and Figure S2, Supporting Information). For a given oil and droplet size, the analytical model indicates that the focal length of the microlens should decrease continuously with the effective refractive of the droplet, n_{eff} (Figure 4e). To complement this theoretical model, we performed finite element simulations on a representative droplet illuminated with monochromatic collimated light (Figure 4f and Figure S3, Supporting Information). The simulations confirm that the droplet diverges the incoming light, leading to a focal point positioned between the droplet and light source, as observed in the experiments (Figure 4g and Figure S3, Supporting Information). Changes in the refractive index of the droplet results in a shift of the simulated focal length, in close agreement to the analytical model (Figure 4e). By exploring other materials and droplet types, the simulations provide useful guidelines for the design of the droplet-based microlens (Figure S4, Supporting Information).
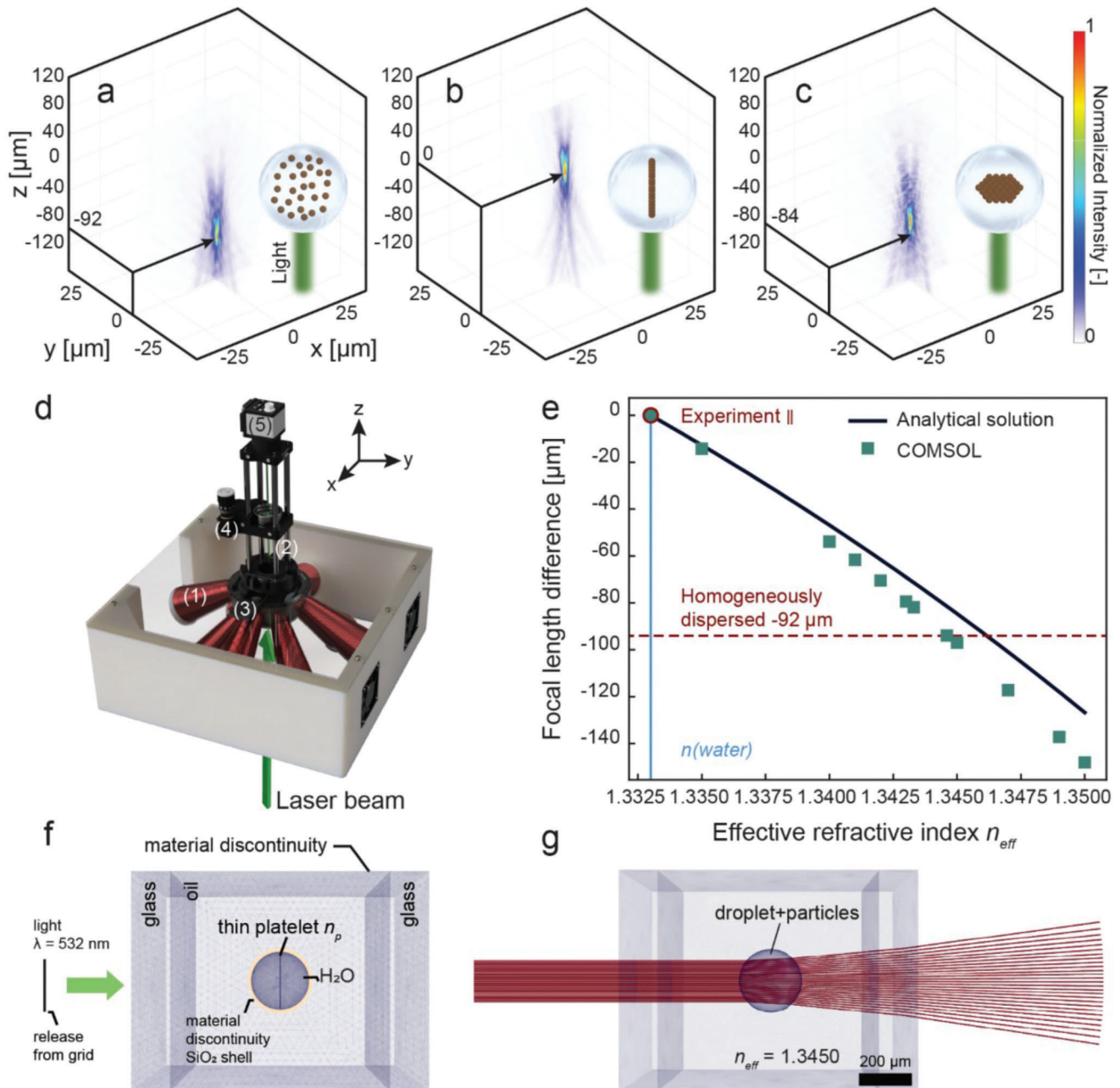
Figure 4. Active microlenses comprising water-in-oil droplets loaded with magnetically responsive superparamagnetic polystyrene colloids. a–c) Maps of the experimentally measured light intensity spatial distribution resulting from the refraction by droplets containing colloids in different configurations: a) homogeneously dispersed superparamagnetic polystyrene particles (no magnetic field), b) colloidal cluster oriented with its plane parallel to the laser beam, and c) colloidal cluster oriented with its plane perpendicular to the laser beam. d) Rendering of the optical setup used to measure the change in focal length of individual droplet-based lenses under the action of a magnetic field. The individual components of the setup are: 1) magnetic coils, 2) laser beam, 3) sample, 4) UV lens mounted on a z-axis translational lens mount, and 5) detector. e) Effect of the effective refractive index of the droplet on the change in focal length using a colloid-free water droplet as reference. Experimental data is shown in red, green squares indicate results from ray tracing simulations, and the black line is the analytical solution. f) Illustration of the 3D ray optics model used for the finite element simulations, including boundary and ray release conditions. g) Simulated ray trajectories ($\lambda = 532$ nm) for a homogeneously dispersed suspension of particles with effective refractive index of $n_{eff} = 1.3450$, corresponding to a change in focal length of -92 μm as measured in the experiment.
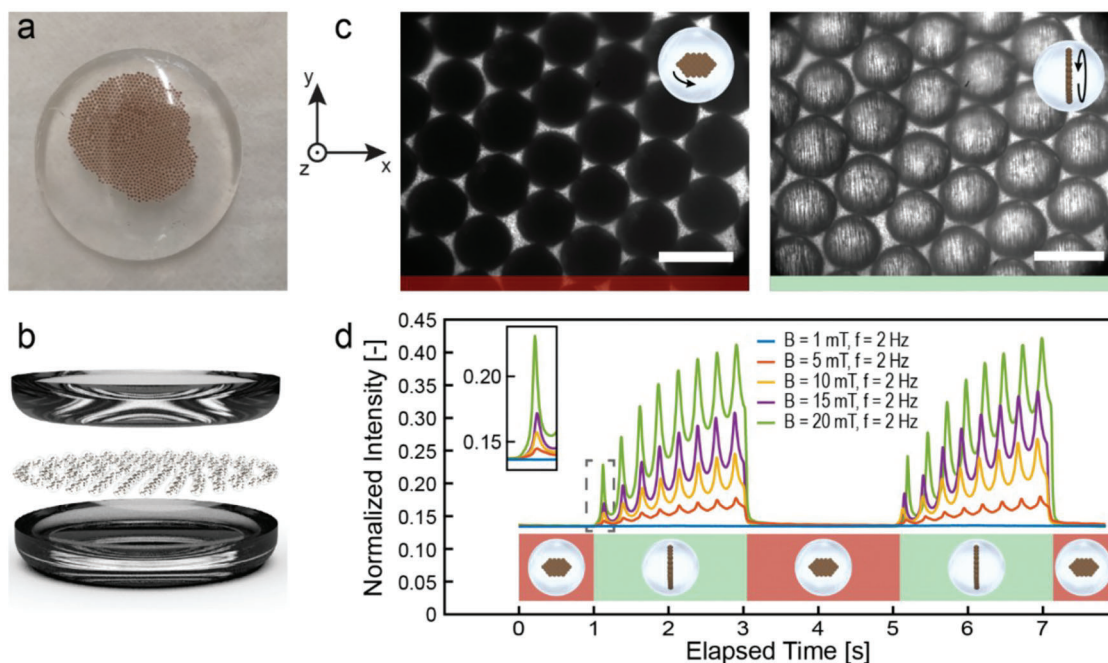
Figure 5. Droplet-based optical shutter controlled by magnetic fields. a) Photograph of a polymer monolith containing colloid-laden water droplets. b) Rendered sketch showing the manufacturing steps of the optical shutter (see Figure S5, Supporting Information). c) Optical microscopy images displaying the color of the droplets when the shutter is ON (left) and OFF (right). A flux field of 20 mT is applied for the OFF and ON states. Scale bar is 500 µm. d) Intensity of light transmitted across the droplet array when the shutter is subjected to consecutive ON/OFF cycles. The ON state is reached when the magnetic field is rotated within the *xy*-plane, whereas the OFF state is achieved when the applied field rotates within the *yz*-plane. The experimental data depict the effect of the magnetic flux density at a fixed frequency of 2 Hz.

The simulations and the analytical model suggest that the focal length change observed when the parallel-aligned clusters (state 2) disperse into homogeneously distributed colloids (state 1) can be explained by a change in the effective refractive index of the droplet. Assuming that the refractive index of the droplet with the parallel-oriented cluster is dominated by water (n_{eff} = 1.330, red circle in Figure 4e), our simulation predicts that the effective refractive index of the droplet should increase to 1.345 for the homogeneously suspended colloids (dashed line, Figure 4e). While the magnetic nature of the suspended colloids prevents us from estimating the effective refractive index of the homogeneous droplet, the higher refractive index of polystyrene (n = 1.58) compared to water makes our physical interpretation a reasonable qualitative explanation for the experimental observations. Because of the heterogeneous nature of droplets with perpendicularly aligned clusters, we expect the focal length change induced by this configuration to arise from the complex interactions of the beam with the particles within the oriented cluster.

Compared to previous work on gravity-dominated droplet microlenses,[38] our system enables deliberate control over the light focusing effect through the use of an external magnetic field. This comes at the cost of a lower optical transparency of the liquid droplet. The ability to control the droplet magnetically is also an advantage compared to lipid droplets naturally present in living cells, which require optical tweezers with potential phototoxic effects for droplet manipulation inside cells.[39] However, our magnetic-driven droplets, in their current form, are too large to be incorporated in living cells for real-time monitoring of biologi-

cal processes. Together, these distinct droplet-based microlensing approaches provide a broad range of tools for the manipulation of light in synthetic and biological systems.

In addition to microlens arrays, the colloid-laden droplets can also be exploited as magnetically controlled optical shutters. We provide an example of such an application by preparing a demonstrator that consists of a polymer monolith containing a monolayer of water droplets (**Figure 5**a,b). The monolith is made by using an oil continuous phase that can be polymerized after the assembly of the microfluidic droplets (Figure S5, Supporting Information). Although the optical shutter can also be fabricated by keeping the continuous phase fluid, the polymerization of this liquid to form a polymer monolith makes the device more mechanically robust.

For the fabrication of the optical shutter, a high concentration of superparamagnetic particles of 1.95 vol% is used in order to amplify the difference in light transmission through the monolith when the shutter is in the ON and OFF states. This particle content is above the minimum concentration of 0.39 vol% that we experimentally found to be necessary to generate a significant magnetically induced change in light transmission. A rotating magnetic field is applied to assemble the particles into anisotropic structures aligned either perpendicular or parallel to the incoming light, thus switching the shutter ON or OFF, respectively. By using a low rotational frequency up to 5 Hz, we expect the particles to assemble into oriented chains and clusters under the applied field. Such frequency is lower than the critical value needed to form the 2D clusters observed in the droplet-based microlenses.

**ADVANCED
SCIENCE NEWS**

www.advancedsciencenews.com

**ADVANCED
OPTICAL
MATERIALS**

www.advopticalmat.de

The performance of the optical shutter was assessed by measuring the evolution of the transmitted light while the plane of the rotating magnetic field was periodically changed between the parallel and perpendicular orientations. Experiments were carried out under an optical microscope using magnetic flux density magnitudes in the range 1–20 mT. The transmitted light intensity was obtained directly from optical microscopy images using image analysis software (Figure 5c,d).

Our results reveal that the transmitted light intensity can change up to twofold when the plane of the rotating magnetic field is switched between the perpendicular and parallel orientations (Figure 5c). Images of the droplet when exposed to the parallel field orientation confirm the assembly of the particles into multiple anisotropic structures, the alignment of which favors light transmission. When the field is changed to the perpendicular orientation, the anisotropic colloidal structures are no longer visible due to complete blockage of the incoming light. The oscillations in transmitted light observed in the OFF state match the frequency of the applied magnetic field (Figure 5d and Figure S6, Supporting Information) and probably result from the oblate geometry of the colloidal clusters. This suggests that the magnetically assembled structures oscillate around the plane of the magnetic field despite being locked in the imposed orientation.

The timescale of the light intensity changes depends on the switching direction and on the magnitude of the magnetic field. Switching the shutter from OFF to ON (darkening effect) happens at a speed that depends on the magnetic field applied. The time it takes to switch from the maximum to the minimum intensity value for field flux densities of 5, 10, 15, and 20 mT are 0.07, 0.15, 0.25, and 0.25 s, respectively. Larger applied magnetic fields lead to higher maximum intensity values, resulting in longer time intervals for them to return to their baseline transmittance levels. The effect of the magnetic field strength on the switching time is reversed when we consider the switching from the ON to the OFF states (whitening effect). In this case, the duration necessary to increase the intensity to a certain fixed level decreases with the magnitude of the magnetic field. When a magnetic flux density of 10 mT is applied, it takes 2 s to increase the light transmittance above 20%. However, when a field amplitude of 20 mT is used, the same intensity value can be attained in only 0.45 s. The strongest whitening effect leads to a 30% rise in light transmittance from the baseline. This is achieved through the application of a magnetic flux density of 20 mT and a rotational frequency of 1 Hz (see Supporting Information and Figure S6, Supporting Information). The long timescales needed to transition from the ON to the OFF state might result from the relatively slow process of merger of small initial particle chains into larger anisotropic structures. These experimental results provide insights into the several parameters governing the dynamics of the magnetic assembly process. Future research should be dedicated to further explore this parameter space and thus tune the switching timescales to meet technological demands.

The proof-of-concept devices shown here illustrate the potential of magnetically driven droplet-based systems for the manipulation of light using a controllable external field. Several other possibilities can be envisioned by further exploring the rich complexity of multiple emulsions and colloidal particle assemblies. For example, structural color can be produced by crystallizing the colloidal particles into multilayered ordered clusters under the action of a rotating magnetic field. Preliminary experiments confirm the magnetically induced formation of such colloidal crystals (Figure S7 and Movie S3, Supporting Information), the color of which can be tuned by rotating the particle cluster. Another possible strategy to manipulate light is to incorporate the magnetic polystyrene particles in microfluidic multiple emulsions.[40] The multiple layers of the emulsion droplet could refract light in a similar way to microstructured solid particles,[41,42] creating a complex 3D focusing field that can be dynamically shaped by the external magnetic field.

3. Conclusions

Superparamagnetic colloids inside droplets can be harnessed to create droplet-based microlenses and optical shutters driven by low-magnitude magnetic fields (6–12 mT). In the presence of a rotating magnetic field, the colloids assemble into tunable 2D clusters driven by the line tension arising from the alignment of magnetic dipoles at the edge of the cluster. The cluster comprises one layer of superparamagnetic polystyrene colloids and can easily vary between 50 and 250 μm in diameter, depending on the droplet size and the initial particle concentration in the droplet. Increasing the applied magnetic field strength enhances the line tension, resulting in smaller and stiffer clusters. Clusters can be manipulated by revolving the applied rotating field below a critical frequency. Such a critical frequency scales with the square of the applied field, as predicted by a balance of viscous and magnetic torques acting on the cluster. The ability to assemble and manipulate the 2D colloidal clusters allows one to change the effective refractive index of the droplet and thereby shift the focal length of magnetically controlled droplet-based microlenses. Alternatively, the assembly of colloids into clusters can be used to change the transmittance of light through the droplet, thus leading to magnetically driven optical shutters. In addition to these proof-of-concept demonstrators, the proposed encapsulated colloids may find potential applications in bioinspired color-changing displays, optical devices for telecommunications, camouflage skins, and magnetically writable boards.

4. Experimental Section

Manufacturing of Microfluidic Devices: Glass microfluidic devices were fabricated using wet etching techniques previously reported in the literature.[43] Briefly, two 1.0 mm thick borosilicate glass wafers (Borofloat 33 Schott) were annealed for 4 h at 580 °C to remove any internal stresses caused by the polishing during production. 50 nm Cr and 50 nm Au thick layers were deposited on the glass substrates using electron beam physical vapor deposition. The wafers were spin-coated with a negative photoresist (AZ10XT 520 cp, thickness of 8 μm) and templated with a sequence of photolithography steps. Both wafers were chemically etched in 40% HF at an etching rate of 3.2 μm min^{-1}. The flow-focusing device was etched to a depth of 120 μm, while for the open step emulsification device channels 100 μm deep were produced. Following the etching step, the mask was removed in succession using acetone, isopropanol, gold etchant, and chrome etchant. The wafers were diced into 15 × 30 mm^2 (flow-focusing) or 15 × 50 mm^2 (step emulsification) chips and 0.7 mm inlets were drilled using a diamond-coated drill bit. Next, the wafers were meticulously cleaned with acetone and isopropanol, and subjected to two surface activation steps, first in piranha (1:1, sulfuric acid:hydrogen peroxide) and later in RCA1 (1:1:5, ammonium hydroxide:hydrogen peroxide:water) solutions. After such treatments, the wafers were flushed with

**ADVANCED
SCIENCE NEWS**

www.advancedsciencenews.com

**ADVANCED
OPTICAL
MATERIALS**

www.advopticalmat.de

water and manually aligned while still wet. Weakly bonded chips were obtained after drying for several hours. A stronger connection was achieved by thermal bonding of two symmetric glass wafers for 4 h in a furnace at a temperature of 620 °C, which was slightly above the glass transition temperature (T_g) of borosilicate glass. To ensure good contact between the two wafers, weights were placed on top of each chip, resulting in an applied pressure of 22 (15×30 mm^2) and 26 kPa (15×50 mm^2). The success of the bonding step was controlled by visual inspection under an optical microscope.

Surface Treatment of Microfluidic Channels: The microfluidic device was connected to plastic syringes (BD Luer-Lok Syringe), mounted on displacement-controlled pumps (Pump 33 DDS, Harvard Apparatus), using PTFE tubing (outer diameter of 1.6 mm, inner diameter of 0.8 mm, Bohlender) and a 4-way linear connector (Dolomite Microfluidics).

To form water-in-water-in-oil or water-in-oil emulsion droplets, the channels of the microfluidic devices need to be surface treated to become hydrophobic. To prepare for such surface treatment, the devices were cleaned in a furnace (model LT 5/11/B410, Nabertherm) at 550 °C for 4 h, then flushed with 1 M NaOH and rinsed with water. The functionalization was performed by flowing a toluene solution containing 5 vol% octadecyltrimethoxysilane (Acros) and 0.5 vol% butyl amine (Acros) for 2 h at a flow rate of 100 µL h^{-1}.

Microfluidic Emulsification: Water droplets loaded with magnetic polystyrene particles were prepared by microfluidic emulsification. Monodisperse magnetic responsive polystyrene nanoparticles were purchased from MicroParticles GmbH (PS-MAG-COOH). The as-received particles show a mean diameter of 536 nm and contain COOH functional groups on the surface. The polystyrene was loaded with an iron oxide content >30 wt% and the surface functionalized with carboxyl groups. The particles were supplied as a suspension with 1.95 vol% solid content. Such dispersion was either used as received or diluted with Milli-Q water at different concentrations ranging from 0.01 vol% up to 0.78 vol% and used as dispersed phase of the emulsions.

Unless mentioned otherwise, the water droplets were covered with silica nanoparticles to form highly stable Pickering emulsions. The silica nanoparticles were suspended in water and delivered as a co-flowing aqueous middle phase during the emulsification process (Figure 2, main text). The suspensions contained 10 vol% silica nanoparticles with a mean diameter 120 nm (SNOWTEX ZL, Nissan Chemicals). The particles were partially hydrophobized with hexyl amine (Acros) to a calculated SiOR surface density of 3.22 nm^{-1} before dilution to a concentration of 1.5 vol% to be used as the middle phase. For all the experiments, the flow rates of the dispersed and middle phases were set to 600 and 300 µL h^{-1}, respectively. This leads to a theoretical surface coverage of around three monolayers. The long serpentine channel in the chip was designed to give the silica nanoparticles enough time to diffuse and adsorb at the water/oil interface.

The continuous phase of the emulsions was formulated depending on the targeted experiments or demonstrations. For the experiments on the assembly and fragmentation dynamics of 2D colloidal clusters, the nonionic surfactant cetyl PEG/PPG-10/1 dimethicone (ABIL 90 EM, kindly provided by Evonik) was dissolved in 1-decanol at a concentration of 2 wt% and used as continuous phase. This non-aqueous surfactant solution was also employed for the demonstration of magnetically controlled active lenses. For the magnetic shutter experiments, 2 wt% polyglycerol polyricinoleate (PGPR 4150, kindly provided by Palsgaard) was used as surfactant in the oil phase, which consisted of isodecyl methacrylate (Sigma-Aldrich) and 1,6-hexanediol dimethacrylate (TCI) with a weight ratio of 7:3 and 1 wt% 2,4,6-trimethylbenzoyldiphenyl phosphine oxide (Sigma-Aldrich) as photoinitiator. Because the continuous phase was polymerized right after emulsification, no Pickering stabilization with silica nanoparticles was employed for the fabrication of the magnetic shutters. For this set of experiments, a step emulsification glass microfluidic device with 100 µm step height was employed.

Magnetic Alignment Setup: The assembly and manipulation of the magnetic responsive nanoparticles were performed using the magnetic system MFG-100 from MagnetobotiX, which generates arbitrary magnetic flux densities up to 20 mT at frequencies up to 2 kHz. As described in previous work,[44] the arrangement of eight electromagnets into two sets allows for unrestrained rotational freedom of the magnetic field. This was accomplished by the superposition of multiple magnetic fields, which creates a homogeneous magnetic field within a spherical workspace with a diameter of ≈10 mm. The coils of the magnetic system featured a soft magnetic core (Vacoflux50) which offers negligible remanence and allows for linear superposition below saturation. Imaging of the colloidal manipulation was performed using an inverted optical microscope (DM IL LED, Leica) equipped with a Leica DFC 295 camera.

Magnetic Assembly and Manipulation: Monodisperse droplets containing defined concentrations of magnetic polystyrene particles were prepared to study the assembly and fragmentation dynamics of 2D superparamagnetic colloidal clusters. To investigate the role of the magnetic field density and rotational frequency ($f_{formation}$) over the size of the assembled colloidal clusters, a monolayer of monodispersed droplets containing magnetic responsive particles was deposited on a microscope well slide. The glass surface of the slide was modified to be hydrophobic using a solution containing 5 vol% octadecyltrimethoxysilane and 0.5 vol% butyl amine in toluene. A cover slip was placed on top of the slide to seal the well and reduce the evaporation of 1-decanol. The colloids were assembled into a single cluster using the manual controls of the magnetic setup (pitch, yaw, roll) at a fixed magnetic flux density of 10 mT and a rotational frequency of 30 Hz. It was experimentally found that this relatively low frequency allowed for a faster formation of a single 2D cluster compared to the higher frequency ($f_{formation}$) of 125 Hz. Control experiments confirmed that the structure and size of the cluster formed at 30 Hz were the same as that obtained at 125 Hz after long times. Once shaped, a rotational magnetic field was applied within the *xy*-plane to manipulate the colloidal clusters (Figure 1, main text). The magnetic flux density ranged from 6 to 12 mT with a rotational frequency ($f_{formation}$) of 125 Hz and a time step between current pulses of 2 ms. The pulse of 2 ms was equivalent to the time it takes for the magnetic field to cover one quarter of a rotating cycle. The concentration of particles in the droplets was varied from 0.02 to 0.078 vol%. For the fragmentation analysis, clusters with three different approximate diameters were studied: 50, 70, and 100 µm. To facilitate visualization, the clusters were rotated around the *x*-axis, so that the edge of the clusters pointed in the direction of the observation field. To study the stability of the 2D colloidal assembly, the rotational plane of the clusters was revolved around the *z*-axis at angular velocities increasing from 0.314 to 2.93 rad s^{-1}. For angular velocities between 0.3 and 1.15 rad s^{-1} the increment was set to 0.1 rad s^{-1}, while from 1.15 to 2.93 rad s^{-1} the velocity was increased by 0.05 rad s^{-1} every revolution. The critical angular velocity at which fragmentation took place was recorded for each cluster inside the droplets.

Active Optical Elements: The active microlenses array was manufactured by collecting a monolayer of monodisperse droplets on a microscope cover slip (#1.5, $n = 1.523$,[45] VWR), which was previously glued on a 3D printed holder (Figure S1, Supporting Information). A 1 mm spacer was placed around the emulsion and covered with a second cover slip (#1.5, $n = 1.523$ [Hibbs A.R., 2006], VWR) to remove the liquid meniscus and to reduce evaporation. The droplets were 271 µm in diameter (coefficient of variation, CV = 1.5%) and contained 0.1061 vol% of magnetic particles. The effective refractive index of the magnetic particles and of the homogeneous particle suspension was calculated using a simple mixing rule. The profile of the light transmitted through the droplets was analyzed using an optical setup comprising a collimated laser beam with a wavelength of 532 nm, a fused silica lens (focal length 50 mm, Thorlabs) mounted on a *z*-axis translational lens mount (SM1ZA, Thorlabs), a 20× magnification objective (Olympus) and a CMOS camera (DCC3260M, Thorlabs). The setup was aligned using 30 mm cage components (Thorlabs) and a 3D printed connector attached to the magnetic setup.

The magnetically driven optical shutter was fabricated using a customized 3D printed container for the assembly and polymerization of the emulsion with a monolayer of droplets (Figure S5, Supporting Information). To facilitate bottom-up photopolymerization, the printed container was attached to a transparent glass slide. The container featured a PDMS layer for easy detachment of the polymerized sample and incorporated a Teflon tube integrated within the 3D printed component to contain the emulsion. The sample was fabricated by depositing a monolayer

**ADVANCED
SCIENCE NEWS**

www.advancedsciencenews.com

**ADVANCED
OPTICAL
MATERIALS**

www.advopticalmat.de

of droplets on a layer of polymerized continuous phase inside the assembled container. The emulsion layer was then solidified through photopolymerization (Figure S5b, Supporting Information) using a UV light source (Omnicure Series 1000, wavelength range 320–500 nm) with an irradiance of 93 mW cm^{-2} in a N$_2$ atmosphere for 10 min. The droplets were 401.7 µm in diameter (CV 8.3%) and contained 1.95 vol% of magnetic particles. To investigate the change in transmittance of the droplets under an external trigger, rotating magnetic flux densities in the range of 1–20 mT and frequencies between 1 and 5 Hz were applied. A sequence of rotational magnetic fields was applied, first revolving on the xy-plane for 2 s and later on the yz-plane for 2 s. The transmittance intensity was measured as a function of time to quantify the response of the magnetic shutter.

Supporting Information

Supporting Information is available from the Wiley Online Library or from the author.

Acknowledgements

Conflict of Interest

Simone Schuerle is co-founder and Member of the Board of MagnebotiX AG.

Data Availability Statement

The data that support the findings of this study are available from the corresponding author upon reasonable request.

Keywords

[1] W. Hu, G. Z. Lum, M. Mastrangeli, M. Sitti, *Nature* **2018**, *554*, 81.
[2] V. F. Cardoso, A. Francesko, C. Ribeiro, M. Bañobre-López, P. Martins, S. Lanceros-Mendez, *Adv. Healthcare Mater.* **2018**, *7*, 1700845.
[3] R. M. Erb, R. Libanori, N. Rothfuchs, A. R. Studart, *Science* **2012**, *335*, 199.
[4] M. A. M. Gijs, F. Lacharme, U. Lehmann, *Chem. Rev.* **2010**, *110*, 1518.
[5] Y. Kim, H. Yuk, R. Zhao, S. A. Chester, X. Zhao, *Nature* **2018**, *558*, 274.
[6] X. Dong, G. Z. Lum, W. Hu, R. Zhang, Z. Ren, P. R. Onck, M. Sitti, *Sci. Adv.* **2020**, *6*, eabc9323.
[7] A. F. Demirörs, S. Aykut, S. Ganzeboom, Y. A. Meier, E. Poloni, *Proc. Natl. Acad. Sci. U. S. A.* **2021**, *118*, e2111291118.
[8] A. F. Demirörs, S. Aykut, S. Ganzeboom, Y. A. Meier, R. Hardeman, J. de Graaf, A. J. T. M. Mathijssen, E. Poloni, J. A. Carpenter, C. Ünlü, D. Zenhäusern, *Adv. Sci.* **2021**, *8*, 2102510.
[9] E. Amstad, M. Textor, E. Reimhult, *Nanoscale* **2011**, *3*, 2819.
[10] D. Kokkinis, M. Schaffner, A. R. Studart, *Nat. Commun.* **2015**, *6*, 8643.
[11] M. D. Banea, L. F. M. da Silva, R. J. C. Carbas, *Int. J. Adhes. Adhes.* **2015**, *59*, 14.
[12] O. Olsvik, T. Popovic, E. Skjerve, K. S. Cudjoe, E. Hornes, J. Ugelstad, M. Uhlén, *Clin. Microbiol. Rev.* **1994**, *7*, 43.
[13] A. Spatafora-Salazar, D. M. Lobmeyer, L. H. P. Cunha, K. Joshi, S. L. Biswal, *Soft Matter* **2021**, *17*, 1120.
[14] P. Tierno, R. Muruganathan, T. M. Fischer, *Phys. Rev. Lett.* **2007**, *98*, 028301.
[15] T. G. Kang, M. A. Hulsen, P. D. Anderson, J. M. J. den Toonder, H. E. H. Meijer, *Phys. Rev. E* **2007**, *76*, 066303.
[16] R. Dreyfus, J. Baudry, M. L. Roper, M. Fermigier, H. A. Stone, J. Bibette, *Nature* **2005**, *437*, 862.
[17] T. Yang, T. O. Tasci, K. B. Neeves, N. Wu, D. W. M. Marr, *Langmuir* **2017**, *33*, 5932.
[18] C. E. Sing, L. Schmid, M. F. Schneider, T. Franke, A. Alexander-Katz, *Proc. Natl. Acad. Sci. U. S. A.* **2010**, *107*, 535.
[19] J. S. Sander, A. R. Studart, *Langmuir* **2013**, *29*, 15168.
[20] J. Heikenfeld, P. Drzaic, J.-S. Yeo, T. Koch, *J. Soc. Inf. Disp.* **2011**, *19*, 129.
[21] B. Comiskey, J. D. Albert, H. Yoshizawa, J. Jacobson, *Nature* **1998**, *394*, 253.
[22] L. M. Mäthger, E. J. Denton, N. J. Marshall, R. T. Hanlon, *J. R. Soc., Interface* **2009**, *6*, S149.
[23] G. Isapour, M. Lattuada, *Adv. Mater.* **2018**, *30*, 1707069.
[24] J. Yang, H. Lee, S. G. Heo, S. Kang, H. Lee, C. H. Lee, H. Yoon, *Adv. Mater. Technol.* **2019**, *4*, 1900140.
[25] N. A. Spaldin, M. Fiebig, *Science* **2005**, *309*, 391.
[26] Y.-L. Huang, D. Nikonov, C. Addiego, R. V. Chopdekar, B. Prasad, L. Zhang, J. Chatterjee, H.-J. Liu, A. Farhan, Y.-H. Chu, M. Yang, M. Ramesh, Z. Q. Qiu, B. D. Huey, C.-C. Lin, T. Gosavi, J. Íñiguez, J. Bokor, X. Pan, I. Young, L. W. Martin, R. Ramesh, *Nat. Commun.* **2020**, *11*, 2836.
[27] G. Dockx, S. Geisel, D. G. Moore, E. Koos, A. R. Studart, J. Vermant, *Nat. Commun.* **2018**, *9*, 4763.
[28] M. P. Kummer, J. J. Abbott, B. E. Kratochvil, R. Borer, A. Sengul, B. J. Nelson, *IEEE Trans. Robot.* **2010**, *26*, 1006.
[29] B. E. Kratochvil, M. P. Kummer, S. Erni, R. Borer, D. R. Frutiger, S. Schürle, B. J. Nelson, in *Experimental Robotics: The 12th International Symposium on Experimental Robotics* (Eds: O. Khatib, V. Kumar, G. Sukhatme), Springer, Berlin **2014**, pp. 317–329.
[30] E. Hilou, D. Du, S. Kuei, S. L. Biswal, *Phys. Rev. Mater.* **2018**, *2*, 025602.
[31] V. Soni, E. S. Bililign, S. Magkiriadou, S. Sacanna, D. Bartolo, M. J. Shelley, W. T. M. Irvine, *Nat. Phys.* **2019**, *15*, 1188.
[32] M. Elismaili, L. Bécu, H. Xu, D. Gonzalez-Rodriguez, *J. Chem. Phys.* **2021**, *155*, 154902.
[33] R. M. Erb, J. Segmehl, M. Schaffner, A. R. Studart, *Soft Matter* **2013**, *9*, 498.
[34] R. M. Erb, J. Segmehl, M. Charilaou, J. F. Löffler, A. R. Studart, *Soft Matter* **2012**, *8*, 7604.
[35] S. Melle, G. G. Fuller, M. A. Rubio, *Phys. Rev. E* **2000**, *61*, 4111.
[36] I. Petousis, E. Homburg, R. Derks, A. Dietzel, *Lab Chip* **2007**, *7*, 1746.
[37] A. Vázquez-Quesada, T. Franke, M. Ellero, *Phys. Fluids* **2017**, *29*, 032006.

**ADVANCED
SCIENCE NEWS**

www.advancedsciencenews.com

**ADVANCED
OPTICAL
MATERIALS**

www.advopticalmat.de

[38] S. Nagelberg, L. D. Zarzar, N. Nicolas, K. Subramanian, J. A. Kalow, V. Sresht, D. Blankschtein, G. Barbastathis, M. Kreysing, T. M. Swager, M. Kolle, *Nat. Commun.* **2017**, *8*, 14673.

[39] X. Chen, T. Wu, Z. Gong, J. Guo, X. Liu, Y. Zhang, Y. Li, P. Ferraro, B. Li, *Light: Sci. Appl.* **2021**, *10*, 242.

[40] L. Y. Chu, A. S. Utada, R. K. Shah, J. W. Kim, D. A. Weitz, *Angew. Chem., Int. Ed. Engl.* **2007**, *46*, 8970.

[41] Y. Zhou, M. Hong, *Opt. Express* **2021**, *29*, 11121.

[42] Y. Zhou, M. Hong, *Photonics Res.* **2021**, *9*, 1598.

[43] A. Ofner, D. G. Moore, P. A. Rühs, P. Schwendimann, M. Eggersdorfer, E. Amstad, D. A. Weitz, A. R. Studart, *Macromol. Chem. Phys.* **2017**, *218*, 1600472.

[44] S. Schuerle, S. Erni, M. Flink, B. Kratochvil, B. J. Nelson, *IEEE Trans. Magn.* **2013**, *49*, 321.

[45] A. R. Hibbs, G. MacDonald, K. Garsha, in *Handbook Of Biological Confocal Microscopy* (Ed: J. B. Pawley), Springer, Boston, MA **2006**, pp. 650–671.